Published in final edited form as:
J Mol Cell Cardiol. 2012 March ; 52(3): 689–700. doi:10.1016/j.yjmcc.2011.12.013.

Differential activation of valvulogenic, chondrogenic, and osteogenic pathways in mouse models of myxomatous and calcific aortic valve disease

Jonathan D. Cheek[1], **Elaine E. Wirrig**[1], **Christina M. Alfieri**, **Jeanne F. James**, and **Katherine E. Yutzey**[1,*]
The Heart Institute, Cincinnati Children's Hospital Medical Center, Cincinnati, OH 45229

Abstract

Studies of human diseased aortic valves have demonstrated increased expression of genetic markers of valve progenitors and osteogenic differentiation associated with pathogenesis. Three potential mouse models of valve disease were examined for cellular pathology, morphology, and induction of valvulogenic, chondrogenic, and osteogenic markers. *Osteogenesis imperfecta murine* (*Oim*) mice, with a mutation in *Col1a2*, have distal leaflet thickening and increased proteoglycan composition characteristic of myxomatous valve disease. *Periostin* null mice also exhibit dysregulation of the ECM with thickening in the aortic midvalve region, but do not have an overall increase in valve leaflet surface area. *Klotho* null mice are a model for premature aging and exhibit calcific nodules in the aortic valve hinge-region, but do not exhibit leaflet thickening, ECM disorganization, or inflammation. *Oim/oim* mice have increased expression of valve progenitor markers *Twist1*, *Col2a1*, *Mmp13*, *Sox9* and *Hapln1*, in addition to increased *Col10a1* and *Asporin* expression, consistent with increased proteoglycan composition. *Periostin* null aortic valves exhibit relatively normal gene expression with slightly increased expression of *Mmp13* and *Hapln1*. In contrast, *Klotho* null aortic valves have increased expression of *Runx2*, consistent with the calcified phenotype, in addition to increased expression of *Sox9*, *Col10a1*, and *osteopontin*. Together these studies demonstrate that *oim/oim* mice exhibit histological and molecular characteristics of myxomatous valve disease and *Klotho* null mice are a new model for calcific aortic valve disease.

Keywords

Aortic valve disease; valvular interstitial cells; calcification; extracellular matrix; Mouse models of human disease

*Corresponding author: Katherine E. Yutzey, Division of Molecular Cardiovascular Biology, Cincinnati Children's Medical Center ML 7020, 240 Albert Sabin Way, Cincinnati, OH 45229, Tel: 513-636-8340; Fax: 513-636-5958, katherine.yutzey@cchmc.org.
[1]These authors contributed equally to the work

Disclosures:
There are no conflicts to disclose.

Introduction

Heart valve replacement is the second most common cardiac surgery performed in the United States with approximately 100,000 valves replaced per year [1, 2]. Calcific aortic valve disease (CAVD) is the most common type of valve disease, with an occurrance of 2% of the adult population over 65, and >25% of aged adults exhibit thickening of the aortic valves [1, 3]. Myxomatous valve disease, characterized by increased proteoglycan composition, also is prevalent and most commonly affects the mitral valve, but myxoid aortic valves have been reported for connective tissue disorders [4, 5]. Molecular markers of valve development, as well as chondrogenesis and osteogenesis, are expressed in human diseased aortic valves and are differentially regulated in children and adults [6, 7]. However, the potential regenerative or pathogenic functions of these regulatory pathways in valve disease progression have not been identified.

The investigation of valve disease mechanisms and therapeutics has been hindered by the lack of appropriate animal models of aortic valve disease. *Apolipoprotein* (*Apo)E*−/− and *low density lipoprotein receptor* (*Ldlr)*−/− hyperlipidemic mice have been used to examine valve pathogenesis associated with atherosclerotic lesions [8, 9]. In these models, dispersed calcific lesions in the aorta, and to a lesser extent in the aortic valve leafets, occur in the presence of extensive lipid accumulation and inflammation. In humans, mutations in *NOTCH1* are associated with bicuspid aortic valve (BAV) and adult CAVD [10]. Likewise, heterozygous loss of Notch1 in mice leads to dispersed aortic valve calcification with osteogenic gene induction in the absence of inflammation or BAV [11, 12]. *Sox9*+/− mice also exhibit aortic valve calcification associated with reduced proteoglycan gene expression [13, 14]. However, none of these previously reported mouse models has discrete nodular calcification on the fibrosa surface of the valves as occurs in human CAVD [15].

Osteogenesis imperfecta murine (*oim)* mutant mice have a spontaneous mutation in the *Collagen*(*Col)1a2* gene and exhibit bone fragility characteristic of human *osteogenesis imperfecta* (OI) [16]. There is initial evidence that humans with OI or *Col1a2* mutations have a predisposition to aortic valve disease [5, 17]. *Oim/oim* homozygous mutant mice have abnormal myocardial function and collagen structure, but valve abnormalities have not been reported previously [18]. Periostin (Postn) is required for normal heart valve development, and adult mice lacking periostin exhibit valve leaflet thickening and dysregulation of TGFβ-beta signaling [19–21]. There is conflicting data on valve calcification, but periostin deficiency in *ApoE* null mice subjected to a high fat diet leads to increased calcification [20, 22, 23]. *Klotho* null mice exhibit abnormal cell signaling and premature aging [24]. Hearts of *Klotho* null mice exhibit sinoatrial node dysfunction associated with sudden death [25], in addition to increased vascular calcification associated with kidney disease [26]. However, the phenotype of the heart valves has not been fully investigated for *Klotho* null mice. Here we report histological, morphological, and molecular manifestations of heart valve pathology in *oim/oim*, *Postn* null, and *Klotho* null mice.

Materials and Methods

Mice

Oim mice (*Col1a2*^{oim}) were obtained from the Jackson Laboratory (stock number 001815) and genotyped by PCR and restriction enzyme analysis using published methods [16, 27]. Cohorts of WT and homozygous *oim/oim* animals were analyzed at 5 and 10 months of age. *Periostin (Postn)* mutant mice were obtained from Dr. Jeff Molkentin, Cincinnati Children's Medical Center and genotyped by PCR of genomic DNA as originally described [28]. Cohorts of *Postn* null and WT littermates were evaluated at 4–5 and 10 months of age. *Klotho* mutant mice (B6;129S5-*Kl*^{tm1lex}), generated by Lexicon Genetics, were obtained

from the Mutant Mouse Regional Resource Center (MMRRC) at UC Davis (ID number 011732-UCD). The *Kl*$^{tm1lex/tm1lex}$ (*Klotho* null) mice exhibit the originally reported premature aging phenotype and do not survive beyond 2 months of age [24, 25, 29]. *Klotho* null mice and control wild type littermates were evaluated at 6–8 weeks of age. *Apolipoprotein (Apo)E*−/− mice [30] were obtained from Taconic and maintained on a high fat diet (Teklad TD 88137, Harlan) for 20 weeks, starting at 10 weeks of age, for induction of atherosclerotic cardiovascular disease [31]. Adult mice were sacrificed by CO_2 inhalation. All animal procedures were approved and performed in accordance with institutional guidelines.

Histology and antibody staining

Hearts were isolated, fixed in 4% paraformaldehyde, paraffin-embedded, and sectioned as previously described [32]. Histological sections (5 μm) were subjected to hematoxylin and eosin (H&E), von Kossa, Alizarin Red, or Movat's pentachrome histological staining as previously described [7, 33, 34]. Masson's trichrome staining was performed using the Masson's trichrome 2000 kit according to manufacturer's instructions (American Mastertech). Immunostaining for phospho-histone H3 (pHH3) and smooth muscle α-actin (SMA) was performed as previously described [7]. Immunostaining for hyaluronan and proteoglycan link protein 1 (Hapln1) was performed as described in [35]. An antibody against CD68 (Abcam, Ab53444; 1:75 dilution) was used to detect macrophages. Immunostaining for CD68 was detected using an ABC staining system (Santa Cruz Biotech, sc-2019) and visualized using DAB substrate (Thermo Fisher Sci). Secondary antibodies used for immunofluorescence include goat anti-mouse alexa-568 (Invitrogen, A11004), goat anti-rabbit alexa-568 (Invitrogen, A11011), and goat anti-mouse alexa-488 (Invitrogen, A11001). Nuclei were stained with ToPro3-642/661 (Invitrogen T3605) according to manufacturer's instructions. Immunofluorescence was imaged using a Nikon A1-R confocal microscope and NIS-Elements D3.2 software. The proliferative index of pHH3 stained nuclei/total nuclei and cell density of total nuclei/leaflet area were quantified on confocal images of 3 sections of n=3 specimens of each genotype using NIS-Elements D3.2 software.

Morphometry

Aortic valve leaflet thickness and area were determined from histologically-stained sections using ImageJ morphometric analysis as previously described [34]. The proximal thickness was measured at the widest point of the hinge region, the middle thickness was measured at the thinnest aspect of the middle third of the valve, and the distal thickness was measured at the widest point of the distal third or tip of the valve. ECM content was quantified in Movat's pentachrome stained sections as the percent area of yellow staining (collagen) or blue staining (proteoglycan) determined using NIS-Elements Basic Research software (Nikon). Images were white balanced, and the valve region (no annulus) was highlighted using the Region of Interest (ROI) tool. RGB values were determined for the range of yellows and blues apparent in the staining, and the threshold was set for each image. Percent area was determined as a ratio of positive pixels within the ROI/total pixels within the ROI. Sample sizes for these analyses were n=5 for WT (*oim*), n=7 for *oim/oim*; n=3 for *Postn* null and WT littermates, n=4 for *Klotho* null and WT littermates. The area of Hapln1 immunostaining in aortic valve leaflets was quantified in photomicrographs as the ratio of positive pixels/total pixels within the ROI based on green RGB threshold values for n=3 animals per genotype using NIS-Elements software. The area of calcification was determined using NIS-Elements D3.2 software in three independent histological sections of the calcified regions of *Klotho* null aortic valves at 6 (n=6) or 8 (n=4) weeks of age. Statistical significance of observed differences between cohorts of mutant and control hearts was determined by paired student's t-tests, $p<0.05$ or $p<0.01$ as indicated.

Quantitative RT-PCR

The aortic valve and surrounding tissue containing the leaflets, annulus, and aortic root were manually dissected from individual adult mouse hearts and placed in Trizol reagent (Invitrogen). After genotyping, tissue from 2–3 mice of the same genotype was pooled and RNA isolated using standard protocols [36]. 200–400 ng RNA was used to generate cDNA, and qRT-PCR was performed as previously described [36, 37]. Primers and annealing temperatures for *Twist1*, *Col1a1*, and *asporin* were used as described in [36]. Primers and annealing temperatures for *Col2a1*, *Col3a1*, *matrix metalloproteinase* (*Mmp)13*, and *Postn* are as described in [37]. Published primer sequences were used for amplification of *osteopontin (OPN)*, *alkaline phosphatase (ALP)*, and *bone sialoprotein* (*BSP*) [38]. *Col10a1* was amplified with primers: forward 5′-ACCAGGAATGCCTTGTTCTC-3′ and reverse: 5′-CATAAAGGGCCCACTTGCTA-3′, and *Hapln1* was amplified with primers: forward: 5′-TCAGGAACTACGGGTTTTGG-3′ and reverse: 5′-AAGCTTCCAGGCAGCAAATA-3′, both at annealing temperatures of 55° C. Standard curves for amplification of each primer pair were generated with 1 μl cDNA derived from 1 μg RNA isolated from mouse E17.5 limbs or from E10.5 or E13.5 whole embryos. Baseline gene expression levels were normalized to L7 expression levels as previously described [36]. Alternatively, RNA expression levels were determined by Taqman gene expression assays and the StepOnePlus system using 1 μl cDNA (Invitrogen). Taqman assays were used for amplification of *Sox9* (Mm00448840_m1), *Runx2* (Mm00501584_m1), *Osteocalcin* (Mm03413826_mH), and *SP7/Osterix* (Mm04209856_m1). Taqman assay gene expression levels were determined by the ΔΔCT method according to manufacturer's instructions (Invitrogen) and normalized to the control gene *beta 2 microglobulin* (B2m) (Mm00437762_m1). Normalized expression levels in the WT cohort for each individual mouse line were set to 1.0 for each gene, and relative expression for corresponding *oim/oim*, *Postn* null and *Klotho* null mice was calculated. Each RNA sample was derived from 2–3 mice of the same genotype, and 3 independent RNA samples (n=3) were analyzed in triplicate for each genotype. Statistical significance of observed differences was determined by paired student's t-tests, $p<0.05$.

Echocardiography

Transthoracic two-dimensional and Doppler echocardiography was performed using a VisualSonics Vevo 770 imaging system with a 30-mHz transducer (Toronto, Canada). Valve performance was evaluated essentially as previously described [34]. *Oim/oim* and *Postn* null mice with appropriate control littermates were evaluated at 5 months of age. *Klotho* null and WT littermates were evaluated at 6–7 weeks of age. Body weights were determined after sacrifice.

Results

Histological assessment of mouse models of aortic valve disease

Histological analysis of sectioned hearts from *oim/oim*, *Postn* null, and *Klotho* null animals was performed to assess valve extracellular matrix (ECM) organization and leaflet morphometry. Aortic valves were examined in detail at histological and molecular levels for each model because the aortic valve is the predominant site of human calcific valve disease. Overall valve morphology was examined by H&E staining, and calcification was detected using von Kossa and Alizarin red stains. ECM composition and organization were assessed using Movat's pentachrome and Masson's trichrome stains. Aortic valve leaflet thickness and area were calculated from histologically-stained sections of hearts for each genotype.

Histological analysis demonstrates that aortic valves from *oim/oim* mice are thickened at the distal tips at 5 months, and further thickening is apparent at 9 months of age (Figure 1B, C arrows). Morphometric analysis demonstrates overall increased aortic valve leaflet area, as

well as increased thickness of the proximal hinge region and distal segments, however the thickness of the medial region is unaffected (Table 1). The *oim* mice are in a B6C3Fe background, and melanocytes are apparent by H&E, as well as von Kossa staining (Figure 1C, F Asterisks), as previously reported for black mice [6]. However, there is no black staining unique to the von Kossa stain, thus indicating a lack of calcification in *oim/oim* mice (Figure 1D–F). The thickening of the distal valve leaflets is primarily due to increased proteoglycan deposition, as indicated by increased blue-green pentrachrome staining (Figure 1H, I, arrows; quantified in Figure S1). The distal thickened region has little fibrillar collagen, as indicated by lack of yellow staining in pentachrome- and diffuse blue staining in trichrome-stained sections (Figure 1H, I, K, L arrows). Thickening also is observed in the valve hinge region with increased proteoglycan contribution, although collagen fibrils remain predominant in this area (Figure 1I, L). In contrast, collagen fibril formation is comparable to controls in the valve leaflet midsection as indicated by both pentachrome and trichrome stains (Figure 1H, I, K, L arrowheads; quantified in Figure S1), and this region is not thickened as indicated by morphometry (Table 1). Interestingly the *oim/oim* mitral valves are relatively unaffected with no apparent increase in valve area or proteoglycan deposition relative to controls (data not shown). This is similar to the human patients with OI in which aortic valve disease is much more prevalent than mitral valve disease [5]. The increase in aortic valve leaflet area and proteoglycan deposition in the *oim/oim* mice is consistent with human myxomatous valve disease pathology.

In contrast to the *oim/oim* valves, *Postn* null aortic valve leaflets are not thickened at the distal and proximal ends, but leaflet thickening is apparent in the valve midsection (Figure 2B, D, F, H; Table 1). No valve calcification was observed by von Kossa staining of *Postn* null hearts at 5 or 10 months. Overall stratification and ECM compartmentalization of the aortic valve leaflets is abnormal in *Postn* null aortic valve leaflets, as indicated by pentachrome and trichrome staining. Fibrillar collagen in the medial section of the valve leaflet is disrupted as indicated by pentachrome staining (Fig 2F, arrows). The alteration in fibrillar collagen in *Postn* null heart valves is consistent with previous reports of mice lacking periostin [20, 28, 39]. In addition, the thickened *Postn* null aortic valve midsection has predominant staining for proteoglycans (Figure 2C–H arrows), but the proximal hinge region is comparable to controls (Figure 2C–H arrowheads). The *Postn* null mitral valves are similarly affected as previously described [21]. At 10 months of age there is no obvious progression of the disease, and the aortic valve medial thickening and altered collagen fibrillogenesis is similar to that observed at 5 months of age (data not shown).

The morphology and ECM organization of *Klotho* null aortic valve leaflets is relatively normal in comparison to control littermates, as indicated by histological and morphometric analysis (Figure 3, Table 1, Figure S1). No significant differences were observed in valve leaflet area or thickness in proximal, middle, or distal regions (Table 1). In addition, proteoglycan distribution and collagen fibrillogenesis are comparable to WT controls in pentachrome- and trichrome-stained sections (Figure 3H, J, quantified in Figure S1). However, nodular calcification is evident in the hinge region of the aortic valves in von Kossa and Alizarin red stained sections (Figure 3D, F insets). The calcification of *Klotho* null valves is localized to the fibrosa layer near the hinge region and extends through several adjacent sections. This pattern of calcification at the point of attachment has been reported for human calcific aortic valve disease [15].

VIC activation, cell proliferation, and cellularity in mouse models of valve pathogenesis

In adult human CAVD, VIC activation occurs with increased expression of myofibroblast markers, such as smooth muscle α-actin (SMA), and increased cell proliferation [7, 40]. Cell proliferation was monitored by pHH3 immunoreactivity in *oim/oim*, *Postn* null and *Klotho* null aortic valves (Figures 4, 5A). As expected, little to no cell proliferation was detected in

normal adult control valves [33]. However, in *oim/oim* aortic valves, increased cell proliferation is present predominantly at the distal tips of the leaflets (Figure 4B). Cell proliferation also is increased in the *Postn* null aortic valves (Figure 5A), but proliferating cells are localized to the interstitial cells of the valve midregion (Figure 4D). In contrast, no differences in cell proliferation were observed in *Klotho* null aortic valves relative to WT control littermates (Figure 4F, 5A). However, age-related differences were noted in the higher indices of aortic valve cell proliferation detected in both the *Klotho* null and WT control littermates evaluated at 6–7 weeks of age, relative to the *oim/oim* and *Postn* null cohorts evaluated at 4–5 months of age. Thus cell proliferation is increased in *oim/oim* and *Postn* null aortic valves, but not in *Klotho* null aortic valves, relative to littermate controls.

SMA expression is not apparent in the pHH3 positive cells in any of the mice (Figure 4, insets), suggesting that myofibroblast activation does not occur with induction of cell proliferation in these animal models. In addition, the cell density is not increased, as indicated by similar total number of nuclei/area, in *oim/oim*, *Postn* null or *Klotho* null aortic valves compared to controls (Figure 5B). Both the *oim/oim* and *Postn* null valves have increased surface area (Table 1), thus the overall cell number is increased, consistent with the observed increase in cell proliferation. SMA expression and localization in *oim/oim* and *Postn* null aortic valves is similar to controls (Figure 4A–D), and no significant differences in the numbers of SMA-positive cells were observed among genotypes (Figure 5C). In *Klotho* null calcified valves, SMA expression is significantly decreased relative to littermate controls (Figure 5C). Thus, myofibroblast activation as indicated by SMA expression is not apparent in *oim/oim*, *Postn* null, or *Klotho* null aortic valves at the stages analyzed.

Expression of valvulogenic, chondrogenic, and osteogenic genes in mouse models of valve disease

The expression of genes associated with valve development, chondrogenesis, and osteogenesis was examined in *oim/oim*, *Postn* null, and *Klotho* null aortic valves. The bHLH transcription factor Twist1 and its target gene *Col2a1* are expressed preferentially in embryonic endocardial cushion valve progenitor cells [37, 41]. Periostin is highly expressed in valve progenitor cells, but its expression is maintained in fetal and adult valves [19, 20, 41]. The matrix remodeling enzyme gene *Mmp13* also is preferentially expressed in the highly proliferative valve progenitor cells and activated myofibroblasts [37, 41, 42]. Analysis of expression of genes associated with valve progenitor cells reveals differences in gene expression consistent with specific valve pathologies (Figure 6A). Expression of the valve progenitor marker *Twist1* is increased only in the *oim/oim* aortic valves, and expression of *Col2a1* also is increased by 3-fold in the *oim/oim* aortic valves. However, *Postn* mRNA expression is not significantly affected in any of the three models. In contrast *Mmp13* expression is increased in all three models with associated induction of ECM remodeling [42]. The increased expression of valve progenitor genes *Twist1* and *Col2a1* in the *oim/oim* model of valve disease is consistent with the overall increased cellularity and matrix deposition that is not apparent in the in *Postn* null or *Klotho* null aortic valves.

Myxomatous valve disease is characterized by increased expression of proteoglycans and hyaluronan-associated genes [43]. Sox9 is a transcription factor required for cartilage development and also is necessary for valve cell proliferation and differentiation [13, 44]. In addition, Sox9 inhibits valve calcification in adult mice [13, 14]. Expression of *Hapln1*, *Col10a1* and *Asporin*, characteristic of cartilage and proteoglycan-rich tissues [36, 45], also was examined in *oim/oim*, *Postn* null, and *Klotho* null aortic valves (Figure 6B). Notably, expression of *Sox9* is increased by 6-fold in *oim/oim* aortic valves, but its expression is not significantly changed in *Postn* null or *Klotho* null aortic valves. Expression of *Hapln1*, *Col10a1*, and *Asporin* also is increased in the *oim/oim* aortic valves, consistent with the increased proteoglycan deposition observed histologically. Therefore, the thickening and

increased proteoglycan deposition in *oim/oim* valves is associated with induction of *Sox9*, *Hapln1*, *Col10a1*, and *Aspn* gene expression.

Expression of osteogenic genes characteristic of tissue calcification was examined in *oim/oim*, *Postn* null, and *Klotho* null aortic valves (Figure 6C). Expression of the transcription factor Runx2, required for bone formation, and the bone differentiation markers *alkaline phosphatase (ALP), osteocalcin (OCN),* and *bone sialoprotein (BSP)* was examined. *Runx2* and is induced in the *Klotho* null aortic valves, consistent with increased valve leaflet calcification observed in the *Klotho* null animals. However no significant differences in gene expression >2-fold were observed in *ALP*, *OCN* or *BSP* levels in *oim/oim*, *Postn* null, or *Klotho* null aortic valves. In addition, no increase in expression of the bone-specific transcription factor *SP7/Osterix* was observed in any of the models. Likewise mRNA expression levels for fibrillar collagens *Col1a1* and *Col3a1* were unchanged in all three models. The most increased gene in the *Klotho* null mice relative to controls as determined by microarray gene expression analysis is *osteopontin* (data not shown). By qRT-PCR, *osteopontin* (*Opn*) gene expression is increased by approximately 11-fold in the *Klotho* null mice relative to controls. Variably increased *osteopontin* gene expression also is observed in the *oim/oim* aortic valves, but *Opn* expression is relatively unaffected in the *Postn* null aortic valves. Together, the specific induction of *Runx2* gene expression in the *Klotho* null mice, that exhibit calcification, supports initiation of an osteogenic gene program, but specific markers of terminally differentiated bone were not highly induced in any of the mice with valve pathogenesis.

Proteoglycan localization in mouse models of valve pathogenesis

The localized expression of the cartilage proteoglycan link protein Hapln1 was examined as an indicator of proteoglycan deposition with potentially protective functions in aortic valve calcification [13, 14, 35]. In normal WT aortic valves, Hapln1 expression is localized to the distal ventricularis surface of the leaflets (Figure 7A, C, E, arrowheads) [35]. In the *oim/oim* aortic valves, Hapln protein expression is increased in the thickened distal and proximal segments of the valves (Figure 7B arrows; quantified in Figure S1). This increased Hapln1 expression is consistent with increased surface area and proteoglycan deposition observed histologically, as well as with increased Hapln1 gene expression as detected by qRT-PCR. Hapln1 protein expression also is increased in the medial thickened region, but not in the relatively normal distal or proximal segments of the *Postn* null aortic valves (Figure 7D, Figure S1). No alteration in Hapln1 protein expression is observed in the *Klotho* null aortic valves (Figure 7F, Figure S1), consistent with apparently normal proteoglycan distribution by pentachrome staining (Figure 3H) and chondrogenic gene expression detected by qRT-PCR (Figure 6B).

Aortic valve leaflet calcification occurs without inflammation in Klotho null mice

In the *Klotho* null animals, aortic valve calcification is localized in nodules at the hinge region on the fibrosa side, similar to human valve pathology (Figure 8). Calcification is progressive, as indicated by a 2.5-fold increase ($p<0.01$) in the average area of aortic valve calcification, from 6 weeks (5657 μm^2) to 8 weeks (14143 μm^2) in the *Klotho* null animals. At 8 weeks, multiple calcific lesions are present in *Klotho* null aortic valves, as demonstrated by strong von Kossa and Alizarin red staining (Figure 8A,B). Human aortic valve calcification often occurs in the context of atherosclerosis and inflammation [46]. Therefore immunoreactivity with CD68 was assessed in order to ascertain the presence of macrophages in the aortic valve calcific lesions of *Klotho* null mice. Little or no CD68 immunoreactivity was detected in regions of calcific nodule formation *Klotho* null aortic valves (Figure 8A–C). Additional indicators of inflammation, including immunostaining for CD3 (T-cells) or Ly6B.2 (neutrophils), as well as gene expression of inflammatory

cytokines, are not induced in *Klotho* null aortic valves (data not shown). As a positive control, strong CD68 immunoreactivity is apparent in the area of the calcified lesion of the atherosclerotic plaque present in the aortic wall near the aortic root of *ApoE* −/− mice maintained on a high fat diet (Figure 8D, D′). Thus the nodular calcification in the aortic valve leaflets of the *Klotho* null mice occurs in the absence of a robust inflammatory response, distinct from cardiovascular calcification resulting from hyperlipidemia.

Echocardiographic assessment of valve function

Heart valve structure and function was examined by echocardiography of *oim/oim* and *Postn* null mice with controls at 5 months of age and of *Klotho* nulls compared to WT littermates at 6–7 weeks of age (Table S1). Aortic and mitral valve dimensions, flow velocities, and pressure gradients were assessed by Doppler interrogation as previously described [34]. No differences in aortic and mitral valve annulus dimensions were detected for *oim/oim* or *Klotho* null animals relative to controls. The aortic valve annulus dimension also was not changed for *Postn* null animals, although the mitral valve annulus and flow velocity was significantly decreased, consistent with a previous report of decreased ventricular function in these animals [28]. Notably, no significant differences were observed in aortic valve flow velocities or pressure gradients in *oim/oim*, *Postn* null or *Klotho* null mice, relative to controls. In addition, no aortic valve regurgitation was appreciated by Doppler interrogation of experimental and control groups. Thus aortic valve function, as detected by echocardiography, is unaffected in all three lines of mice, in contrast to observed differences in morphology, ECM composition, and gene expression.

Discussion

Here we report three mouse models with distinct morphometric, molecular, and cellular aortic valve abnormalities related to human valve disease (summarized in Table S2). *Oim/oim* mice exhibit ECM dysregulation, distal leaflet thickening, increased cell proliferation, and induction of valvulogenic and chondrogenic gene expression. *Postn* null mice exhibit localized thickening in the valve midregion, increased cell proliferation, and induction of genes associated with ECM remodeling. Aortic valves of *Klotho* null mice exhibit nodular calcification and osteogenic gene induction with minimal ECM dysregulation or inflammation. Thus each of these models exhibits unique features and molecular mechanisms of valve pathogenesis. However, a limitation of these mouse models of valve pathogenesis is the lack of aortic valve dysfunction as detected by echocardiography (Table S1) [34]. This observation is consistent with previous reports in which aortic valve pathology, apparent by histology in mouse models, often does not result in compromised function, as indicated by multiple imaging modalities (reviewed in [9, 47]). Likewise, in humans valve dysplasia and histological abnormalities can occur in the absence of functional deficits [46]. Thus examination of the molecular and cellular bases of the distinct aortic valve pathologies in the *oim/oim*, *Postn* null, and *Klotho* null mice will be likely be useful in the future identification of molecular mechanisms and potential treatments for human valve disease.

Human aortic valve disease is highly variable and can be, but is not always, associated with congenital malformations or atherosclerotic vascular disease [2]. Additional causes of aortic valve disease include kidney disease or mutations in ECM genes, but, in many cases, the initial causes of aortic valve disease are unknown [6, 48]. In pediatric and adult human valve disease, expression of transcription factors and ECM genes characteristic of embryonic valve progenitor cells is increased in association with valve interstitial cell (VIC) activation and ECM disorganization [7, 37]. The specific origins of activated VICs or cells expressing valvulogenic markers are unknown. Induction of endothelial to mesenchymal transition (EMT) or incorporation of circulating stem cells have been proposed as potential

regenerative or pathogenic mechanisms linked to VIC activation [49, 50]. Previous studies of human valve pathology and of mice with hyperlipidemia and atherosclerotic cardiovascular disease have described a multistep process of valve calcification including VIC activation and endochondral bone formation [8, 51–53]. CAVD in the *Klotho* null mice occurs in the absence of inflammation and valve thickening, supporting a distinct mechanism for valve calcification. Thus valve disease resulting from distinct etiologies is heterogeneous, likely due to differential activation of regulatory pathways associated with valve development, myofibroblast activation, chondrogenesis, osteogenesis, and inflammation. The identification of new mouse models of aortic valve pathogenesis will facilitate mechanistic studies of these disease processes.

The molecular basis of valve abnormalities in both the *oim/oim* mice, with a mutation of *Col1a2*, and in *Postn* null mice is likely related to collagen fiber dysregulation [39], but the pathogenic sequelae are distinct. Interestingly, the *oim/oim* aortic valves exhibit distal thickening, while the *Postn* null aortic valves are thickened in the leaflet midregion, suggestive of localized effects on valve remodeling in response to collagen dysregulation. Significantly expression of the valve progenitor marker *Twist1* and its downstream target gene *Col2a1* is increased specifically in the *oim/oim* mice and also occurs in human pediatric and adult valve disease associated with increased cell proliferation [7, 37]. However, the cellular origins and functions of the Twist1-expressing cells in human diseased valves or mouse models are not known. In contrast, Twist1 expression is not increased in *Postn* null mice that exhibit increased cell proliferation with aortic valve leaflet thickening localized to the mid region. *Postn* null mice exhibit ECM abnormalities that are not as severe as those observed in the *oim/oim* mice and no calcification or osteogenic gene induction is apparent in either model [20]. Previous reports have provided conflicting evidence for valve calcification in the *Postn* null animals, and additional insults, such as loss of ApoE or exposure to high fat diet, may be required to induce a calcific response [20, 22, 23]. Although both *oim/oim* and *Postn* null mice have valve pathogenesis resulting from collagen dysregulation, the valve leaflet phenotype and molecular indicators of disease are distinct in these models. However, neither model exhibits calcification, demonstrating that the ECM abnormalities alone are not sufficient to induce a calcific response.

Human myxomatous valve disease is characterized by increased VIC proliferation, leaflet thickening, increased proteoglycan expression, and ECM remodeling [42]. These are features of the *oim/oim* mouse model that were not observed in the *Postn* or *Klotho* null mice. Myofibroblast activation indicative of induction of smooth muscle markers also is a feature of human myxomatous valve disease [42]. However, little myofibroblast activation was detected in the *oim/oim* mice, suggesting that this may not be a critical feature of myxomatous disease. However, SMA expression was not evaluated in stages prior to the development of valve ECM abnormalities and thus could be an early indicator of valve pathogenesis, although this remains to be demonstrated. In humans with OI, the aortic valve is most commonly affected, with minimal mitral valve involvement [5]. Similarly mitral valve morphology and ECM composition are relatively normal in *oim/oim* mice relative to leaflet thickening and ECM dysregulation observed in aortic valves. However, unlike human OI patients, aortic valve regurgitation was not observed in the *oim/oim* mice that have obvious aortic valve pathology. Increased proteoglycan expression in *oim/oim* mice is associated with increased *Sox9*, *Hapln1* and *Asporin* expression supporting induction of chondrogenic, but not osteogenic, pathways with myxomatous disease. It is not clear how dysregulation of fibrillar collagen leads to myxomatous valve disease, but the further examination of *oim/oim* mice should be a valuable tool in the definition of aortic valve pathogenic mechanisms.

Aortic valve calcification and osteogenic gene induction was observed specifically in the *Klotho* null mice. Several mouse models with aortic valve calcification including high fat fed *ApoE*−/− [8], *LDLr*$^{-/-}$;*ApoB*$^{100/100}$ [54], *RBPJ*+/− [12] and *Postn*−/− [23] [8] mice, as well as *Notch1*+/− [11, 12] and *Sox9*+/− [13, 14], have been reported previously. Unlike these mice, CAVD in *Klotho* null mice is apparent as calcific nodules at the hinge region similar to calcification nodule formation in humans. Cell proliferation is unaffected and SMA expression is reduced in *Klotho* null calcified valves, suggesting that VIC activation is not a feature of aortic valve calcification in these animals. However, it is possible that VIC activation occurs at earlier stages, prior to the development of calcific lesions. In addition, minimal inflammation or ECM dysregulation occurs in *Klotho* null calcified aortic valves. This is in contrast to the atherosclerotic-related valve disease in *ApoE*−/− or *LDLr*$^{-/-}$;*ApoB*$^{100/100}$ hypercholesterolemic mouse models in which valve leaflet thickening and inflammation are apparent in diseased aortic valves [8, 52, 54]. Thus the progression of calcification in the *Klotho* null animals may represent a novel mechanism, distinct from atherosclerotic disease. Since the *Klotho* gene is not expressed in adult aortic valves (data not shown), it is likely that CAVD in *Klotho* null mice is a secondary effect of multiple age-related pathologies, including severe kidney disease [24, 26]. Chronic kidney disease is associated with CAVD in the human population [55], and the calcific nodules in the *Klotho* null mice are similar to human valve pathology [15]. Thus, further examination of valve pathogenesis in these animals is likely to yield clinically significant information on mechanisms of valve calcification.

The current standard of care for aortic valve disease is replacement with a mechanical or bioprosthetic valve [56]. Limitations of this approach are the necessity for anticoagulation treatment for mechanical valves or immunosuppressive drugs, in addition to the likelihood of reintervention in 5–10 years, for bioprosthetic valves. Furthermore, valve disease often is associated with aging, and valve replacement may not be feasible in frail or elderly individuals. Optimally, deceleration or even reversal of the progression of valve pathogenesis could be achieved by pharmaceutical means, but no such therapies are currently available. In mice, reduction of plasma cholesterol slows the progression of CAVD in a hyperlipidemic model, and CAVD shares osteogenic pathways with atherosclerotic calcification, making statins an attractive therapeutic for CAVD [9, 57, 58]. However, a large clinical trial demonstrated that statin therapy is not effective in reducing progression of CAVD or the need for aortic valve replacement [59]. It is possible that heterogeneity in the origins and pathogenic mechanisms of heart valve disease limits the efficacy of statin treatment for many individuals with CAVD. Therefore the examination of multiple mouse models of aortic valve disease resulting from distinct pathogenic mechanisms may provide critical insights into human valve disease origins, progression, and potential treatments in the future.

Supplementary Material

Refer to Web version on PubMed Central for supplementary material.

Acknowledgments

We thank Robert Hinton and Amy Opoka for technical advice and valuable discussions.

Support

This work was supported by NIH/NHLBI R01HL082716 and NIH R01HL094319 grants to KEY.

Abbreviations

CAVD	Calcific aortic valve disease
BAV	Bicuspid aortic valve
OI	*osteogenesis imperfecta*
pHH3	phospho-histone H3
SMA	Smooth muscle α-actin
ECM	Extracellular matrix
VIC	Valve interstitial cell

References

1. Thom T, Haase N, Rosamond W, Howard VJ, Rumsfeld J, Manolio T, Zheng Z, Flegal K, ODonnell C, Kittner S. Heart disease and stroke statistics--2006 update. A report from the American Heart Association statistics committee and stroke statistics subcommittee. Circulation. 2006; 113:e85–e151. [PubMed: 16407573]
2. Roberts WC, Ko JM. Frequency by decades of unicuspid, bicuspid and tricuspid aortic valves in adults having isolated aortic valve replacement for aortic stenosis, with or without associated aortic regurgitation. Circulation. 2005; 111:920–925. [PubMed: 15710758]
3. Freeman RV, Otto CM. Spectrum of calcific aortic valve disease: pathogenesis, disease progression and treatment strategies. Circulation. 2005; 111:3316–3326. [PubMed: 15967862]
4. Devereux RB, Brown WT, Kramer-Fox R, Sachs BS. Inheritance of mitral valve prolapse: Effect of age and sex on gene expression. Ann Int Med. 1982; 97:826–832. [PubMed: 7149490]
5. Bonita RE, Cohen IS, Berko BA. Valvular heart disease in osteogenesis imperfecta. Echocardiography. 2010; 27:69–73. [PubMed: 19725849]
6. Hinton RB, Yutzey KE. Heart valve structure and function in development and disease. Annu Rev Physiol. 2011; 73:29–46. [PubMed: 20809794]
7. Wirrig EE, Hinton RB, Yutzey KE. Differential expression of cartilage and bone-related proteins in pediatric and adult diseased aortic valves. J Mol Cell Cardiol. 2011; 50:561–569. [PubMed: 21163264]
8. Aikawa E, Nahrendorf M, Sosnovik D, Lok VM, Jaffer FA, Aikawa M, Weissleder R. Multimodality molecular imaging identifies proteolytic and osteogenic activities in early aortic valve disease. Circulation. 2007; 115:377–386. [PubMed: 17224478]
9. Miller JD, Weiss RM, Heistad DD. Calcific aortic valve stenosis: Methods, models, and mechanisms. Circ Res. 2011; 108:1392–1412. [PubMed: 21617136]
10. Garg V, Muth AN, Ransom JF, Schluterman MK, Barnes R, King IN, Grossfeld PD, Srivastava D. Mutations in NOTCH1 cause aortic valve disease. Nature. 2005; 437:270–274. [PubMed: 16025100]
11. Nigam V, Srivastava D. Notch1 represses osteogenic pathways in aortic valve cells. J Mol Cell Cardiol. 2009; 47:828–834. [PubMed: 19695258]
12. Nus M, MacGrogan D, Martinez-Poveda B, Benito Y, Casanova JC, Fernandez-Aviles F, Bermejo J, de la Pompa JL. Diet-induced aortic valve disease in mice haploinsufficient for the Notch pathway effector RBPJK/CSL. Arterioscler Thromb Vasc Biol. 2011; 31:1580–1588. [PubMed: 21493891]
13. Lincoln J, Kist R, Scherer G, Yutzey KE. Sox9 is required for precursor cell expansion and extracellular matrix gene expression. Dev Biol. 2007; 302:376–388. [PubMed: 17064679]
14. Peacock JD, Levay AK, Gillaspie DB, Tao G, Lincoln J. Reduced Sox9 function promotes heart valve calcification phenotypes in vivo. Circ Res. 2010; 106:712–719. [PubMed: 20056916]
15. Thubrikar MJ, Jaffar A, Nolan SP. Patterns of calcific deposits in operatively excised stenotic of purely regurgitant aortic valves and their relation to mechanical stress. Am J Cardiol. 1986; 58:304–308. [PubMed: 3739919]

16. Chipman SD, Sweet HO, McBride DJ, Davisson MT, Marks SC, Shuldiner AR, Wenstrup RJ, Rowe DW, Shapiro JR. Defective proa2(I) collagen synthesis in a recessive mutation in mice: A model of human osteogenesis imperfecta. Proc Natl Acad Sci USA. 1993; 90:1701–1705. [PubMed: 8446583]

17. Malfait F, Symoens S, Coucke P, Nunes L, De Almeida S, De Paepe A. Total absence of the alpha2(I) chain of collagen type I causes a rare form of Ehlers-Danlos syndrome with hypermobility and propensity of cardiac valvular problems. J Med Genet. 2006; 42:e36. [PubMed: 16816023]

18. Weis SM, Emery JL, Becker KD, McBride DJ, Omens JH, McCulloch AD. Myocardial mechanics and collagen structure in the osteogenesis imperfecta murine (oim). Circ Res. 2000; 87:663–669. [PubMed: 11029401]

19. Kruzynska-Frejtag A, Machnicki M, Rogers R, Markwald RR, Conway SJ. Periostin (an osteoblast-specific factor) is expressed within the embryonic mouse heart during valve formation. Mech Dev. 2001; 103:183–188. [PubMed: 11335131]

20. Snider P, Hinton RB, Moreno-Rodriguez R, Wang J, Rogers R, Lindsley A, Li F, Ingram DA, Menick D, Field L, Firulli AB, Molkentin JD, Markwald RR, Conway SJ. Periostin is required for maturation and extracellular matrix stabilization of noncardiomyocyte lineages of the heart. Circ Res. 2008; 102:752–760. [PubMed: 18296617]

21. Norris RA, Moreno-Rodriguez RA, Sugi Y, Hoffman S, Amos J, Hart MM, Potts JD, Goodwin RL, Markwald RR. Periostin regulates atrioventricular valve maturation. Dev Biol. 2008; 316:200–213. [PubMed: 18313657]

22. Tkatchenko TV, Moreno-Rodriguez RA, Conway SJ, Molkentin JD, Markwald RR, Tkatchenko AV. Lack of periostin leads to suppression of Notch1 signaling in calcific aortic valve disease. Physiol Genomics. 2009; 39:160–168. [PubMed: 19723774]

23. Hakuno D, Kimura N, Yoshioka M, Mukai M, Kimura T, Okada Y, Yozu R, Shukunami C, Hiraki Y, Kudo A, Ogawa S, Fukuda K. Periostin advances atherosclerotic and rheumatic cardiac valve degeneration by inducing angiogenesis and MMP production in humans and rodents. J Clin Invest. 2010; 120:2292–2306. [PubMed: 20551517]

24. Kuro-o M, Matsumura Y, Aizawa H, Kawaguchi H, Suga T, Utsugi T, Ohyama Y, Kurabayashi M, Kaname T, Kume E, Iwasaki H, Iida A, Shiraki-Iida T, Nishikawa S, Nagai R, Nabeshima Y. Mutation of the mouse klotho gene leads to a syndrome resembling ageing. Nature. 1997; 390:45–51. [PubMed: 9363890]

25. Takeshita K, Fujimori T, Kurotaki Y, Honjo T, Tsujikawa H, Yasui K, Lee JK, Kamiya K, Kitaichi K, Yamamoto K, Ito M, Kondo T, Iino S, Inden Y, Hirai M, Murohara T, Kodama I, Nabeshima Y. Sinoatrial node dysfunction and early unexpected death of mice with a defect of klotho gene expression. Circulation. 2004; 109:1776–1782. [PubMed: 15037532]

26. Hu MC, Shi M, Zhang J, Quinones H, Griffith C, Kuro-o M, Moe OW. Klotho deficiency causes vascular calcification in chronic kidney disease. J Am Soc Nephrol. 2011; 22:124–136. [PubMed: 21115613]

27. Saban J, King D. PCR genotyping of oim mutant mice. Biotechniques. 1996; 21:190. [PubMed: 8862795]

28. Oka T, Kaiser RA, Melendez J, Hambleton M, Sargent MA, Lorts A, Brunskill EW, Dorn GW, Conway SJ, Aronow BJ, Robbins J, Molkentin JD. Genetic manipulation of periostin expression reveals a role in cardiac hypertrophy and ventricular remodeling. Circ Res. 2007; 101:313–321. [PubMed: 17569887]

29. Nakatani T, Sarraj B, Ohnishi M, Densmore MJ, Taguchi T, Goetz R, Mohammadi M, Lanske B, Razzaque MS. In vivo genetic evidence for klotho-dependent, fibroblast growth factor 23 (Fgf23)-mediated regulation of systemic phosphate homeostasis. FASEB J. 2009; 23:433–441. [PubMed: 18835926]

30. Piedrahita JA, Zhang SH, Hagaman JR, Oliver PM, Maeda N. Generation of mice carrying a mutant apolipoprotein E gene inactivated by gene targeting in embryonic stem cells. Proc Natl Acad Sci USA. 1992; 89:4471–4475. [PubMed: 1584779]

31. Tanaka K, Sata M, Fukuda D, Suematsu Y, Motomura N, Takamoto S, Hirata Y, Nagai R. Age-associated aortic stenosis in apolipoprotein E-deficient mice. J Am Coll Cardiol. 2005; 46:134–141. [PubMed: 15992647]

32. Lincoln J, Alfieri CM, Yutzey KE. Development of heart valve leaflets and supporting apparatus in chicken and mouse embryos. Dev Dyn. 2004; 230:239–250. [PubMed: 15162503]
33. Hinton RB, Lincoln J, Deutsch GH, Osinska H, Manning PB, Benson DW, Yutzey KE. Extracellular matrix remodeling and organization in developing and diseased aortic valves. Circ Res. 2006; 98:1431–1438. [PubMed: 16645142]
34. Hinton RB, Alfieri CM, Witt SA, Glascock BJ, Khoury PR, Benson DW, Yutzey KE. Mouse heart valve structure and function: echocardiographic and morphometric analyses from the fetus through the aged adult. Am J Physiol Heart and Circ Phys. 2008; 294:H2480–2488.
35. Wirrig EE, Snarr BS, Chintalapudi MR, O'Neal JL, Phelps AL, Barth JL, Fresco VM, Kern CB, Mjaatvedt CH, Toole BP, Hoffman S, Trusk TC, Argraves WS, Wessels A. Cartilage link protein (Crtl1), an extracellular matrix component playing an important role in heart development. Dev Biol. 2007; 310:291–303. [PubMed: 17822691]
36. Chakraborty S, Cheek J, Sakthivel B, Aronow BJ, Yutzey KE. Shared gene expression profiles in developing heart valves and osteoblasts. Physiol Genomics. 2008; 35:75–85. [PubMed: 18612084]
37. Chakraborty S, Wirrig EE, Hinton RB, Merrill WH, Spicer DB, Yutzey KE. Twist1 promotes heart valve cell proliferation and extracellular matrix gene expression during development in vivo and is expressed in human diseased aortic valves. Dev Biol. 2010; 347:167–179. [PubMed: 20804746]
38. zur Nieden NI, Kempka G, Ahr HJ. In vitro differentiation of embryonic stem cells into mineralized osteoblasts. Differentiation. 2003; 71:18–27. [PubMed: 12558600]
39. Norris RA, Damon B, Mironov V, Kasyanov V, Ramamurthi A, Moreno-Rodriguez R, Trusk T, Potts JD, Goodwin RL, Davis J, Hoffman S, Wen X, Sugi Y, Kern CB, Mjaatvedt CH, Turner DK, Oka T, Conway SJ, Molkentin JD, Forgacs G, Markwald RR. Periostin regulates collagen fibrillogenesis and the biomechanical properties of connective tissues. J Cell Biochem. 2007; 101:695–711. [PubMed: 17226767]
40. Aikawa E, Whittaker P, Farber M, Mendelson K, Padera RF, Aikawa M, Schoen FJ. Human semilunar cardiac valve remodeling by activated cells from fetus to adult. Circulation. 2006; 113:1344–1352. [PubMed: 16534030]
41. Shelton EL, Yutzey KE. Twist1 function in endocardial cell proliferation, migration, and differentiation during heart valve development. Dev Biol. 2008; 317:282–295. [PubMed: 18353304]
42. Rabkin E, Aikawa M, Stone JR, Fukumoto Y, Libby P, Schoen FJ. Activated interstitial myofibroblasts express catabolic enzymes and mediate matrix remodeling in myxomatous heart valves. Circulation. 2001; 104:2525–2532. [PubMed: 11714645]
43. Gupta V, Barzilla JE, Mendez JS, Stephens EH, Lee EL, Collard CD, Laucirica R, Weigel PH, Grande-Allen KJ. Abundance and localization of proteoglycans and hyaluronan within normal and myxomatous mitral valves. Cardiovasc Pathol. 2009; 18:191–197. [PubMed: 18621549]
44. Bi W, Deng JM, Zhang Z, Behringer RR, de Crombrugghe B. Sox9 is required for cartilage formation. Nat Genet. 1999; 22:85–89. [PubMed: 10319868]
45. Lincoln J, Lange AW, Yutzey KE. Hearts and bones: Shared regulatory mechanisms in heart valve, cartilage, tendon, and bone development. Dev Biol. 2006; 294:292–302. [PubMed: 16643886]
46. Otto CM. Valvular aortic stenosis: disease severity and timing of intervention. J Am Coll Cardiol. 2006; 47:2141–2151. [PubMed: 16750677]
47. Sider KL, Blaser MC, Simmons CA. Animal models of calcific aortic valve disease. Int J Inflamm. 2011; 2011:364310.
48. Maher ER, Young G, Smyth-Walsh B, Pugh S, Curtis JR. Aortic and mitral valve calcification in patients with end-stage renal disease. Lancet. 1987; 2:875–877. [PubMed: 2889080]
49. Visconti RP, Ebihara Y, LaRue AC, Fleming PA, McQuinn TC, Masuya M, Minamiguchi H, Markwald RR, Ogawa M, Drake CJ. An in vivo analysis of hematopoietic stem cell potential: hematopoietic origin of cardiac valve interstitial cells. Circ Res. 2006; 98:690–696. [PubMed: 16456103]
50. Paruchuri S, Yang JH, Aikawa E, Melero-Martin JM, Khan ZA, Loukogeorgakis S, Schoen FJ, Bischoff J. Human pulmonary valve progenitor cells exhibit endothelial/mesenchymal plasticity in response to vascular endothelial growth factor-A and transforming growth factor-beta2. Circ Res. 2006; 99:861–869. [PubMed: 16973908]

51. Mohler ER, Gannon F, Reynolds C, Zimmerman R, Keane MG, Kaplan FS. Bone formation and inflammation in cardiac valves. Circulation. 2001; 103:1522–1528. [PubMed: 11257079]
52. Miller JD, Weiss RM, Serrano KM, Casteneda LE, Brooks RM, Zimmerman K, Heistad DD. Evidence for active regulation of pro-osteogenic signaling in advanced aortic valve disease. Arterioscler Thromb Vasc Biol. 2010; 30:2482–2486. [PubMed: 20864669]
53. Li C, Xu S, Gotlieb AI. The response to valve injury. A paradigm to understand the pathogenesis of heart valve disease. Cardiovasc Pathol. 2011; 20:183–190. [PubMed: 21075649]
54. Weiss RM, Ohashi M, Miller JD, Young SG, Heistad DD. Calcific aortic valve stenosis in old hypercholesterolemic mice. Circulation. 2006; 114:2065–2069. [PubMed: 17075015]
55. Piers LH, Touw HRW, Gansevoort R, Franssen CFM, Oudkerk M, Zijlstra F, Tio RA. Relation of aortic valve and coronary artery calcium in patients with chronic kidney disease to the stage and etiology of the renal disease. Am J Cardiol. 2009; 103:1473–1477. [PubMed: 19427449]
56. Bonow RO, Carabello BA, Kanu C, de Leon AC Jr, Faxon DP, Freed MD, Gaasch WH, Lytle BW, Nishimura RA, O'Gara PT, O'Rourke RA, Otto CM, Shah PM, Shanewise JS, Smith SC Jr, Jacobs AK, Adams CD, Anderson JL, Antman EM, Faxon DP, Fuster V, Halperin JL, Hiratzka LF, Hunt SA, Lytle BW, Nishimura R, Page RL, Riegel B. ACC/AHA 2006 guidelines for the management of patients with valvular heart disease: a report of the American College of Cardiology/American Heart Association Task Force on Practice Guidelines (writing committee to revise the 1998 Guidelines for the Management of Patients With Valvular Heart Disease): developed in collaboration with the Society of Cardiovascular Anesthesiologists: endorsed by the Society for Cardiovascular Angiography and Interventions and the Society of Thoracic Surgeons. Circulation. 2006; 114:e84–231. [PubMed: 16880336]
57. Rajamannan NM, Subramaniam M, Stock SR, Stone NJ, Springett M, Ignatiev KI, McConnell JP, Singh RJ, Bonow RO, Spelsberg TC. Atorvastatin inhibits calcification and enhances nitric oxide synthase production in the hypercholesterolaemic aortic valve. Heart. 2005; 91:806–810. [PubMed: 15894785]
58. Miller JD, Weiss RM, Serrano KM, Brooks RM, Berry CJ, Zimmerman K, Young SG, Heistad DD. Lowering plasma cholesterol levels halts progression of aortic valve disease in mice. Circulation. 2009; 119:2693–2701. [PubMed: 19433756]
59. Rossebo AB, Pedersen TR, Boman K, Brudi P, Chambers JB, Egstrup K, Gerdts E, Gohlke-Barwolf C, Holme I, Kesaniemi YA, Malbecq W, Nienaber CA, Ray S, Skjaerpe T, Wachtell K, Willenheimer R. Intensive lipid lowering with simvastatin and ezetimibe in aortic stenosis. N Engl J Med. 2008; 359:1343–56. [PubMed: 18765433]

Highlights

- Osteogenesis imperfecta mice have myxomatous valve disease
- Klotho null mice have calcific aortic valve disease without inflammation.
- Mouse models have differential expression of valve progenitor, cartilage and bone genes.
- Myxomatous and calcific valve disease in mice can occur without myofibroblast activation.

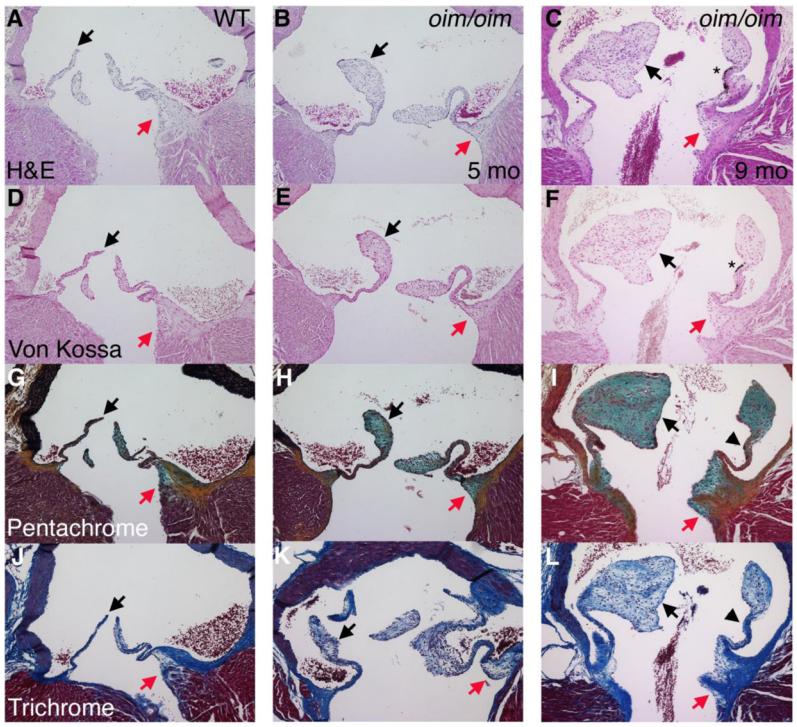

Figure 1. Osteogenesis imperfecta murine (*oim/oim*) aortic valve leaflets exhibit distal thickening and increased proteoglycan deposition

Homozygous *oim/oim* mice with a disease causing mutation in *Collagen1a2* were evaluated at 5 and 9 months of age in comparison to a 5 month-old control littermate. Comparison of H&E (A–C) and von Kossa (D–F) stained sections demonstrates absence of calcification, but presence of black melanocytes (*). Distal thickening of leaflets is indicated by arrows, but the medial valve region (arrowheads) is relatively normal. Movat's pentachrome staining (G–I) indicates increased proteoglycan deposition (aqua) in the distal region with collagen fiber formation (yellow) in the medial region. Masson's trichrome staining (J–L) indicate decreased collagen deposition (blue) in the thickened distal region, but normal collagen in the medial region. Thickening of the hinge region is indicated by red arrows.

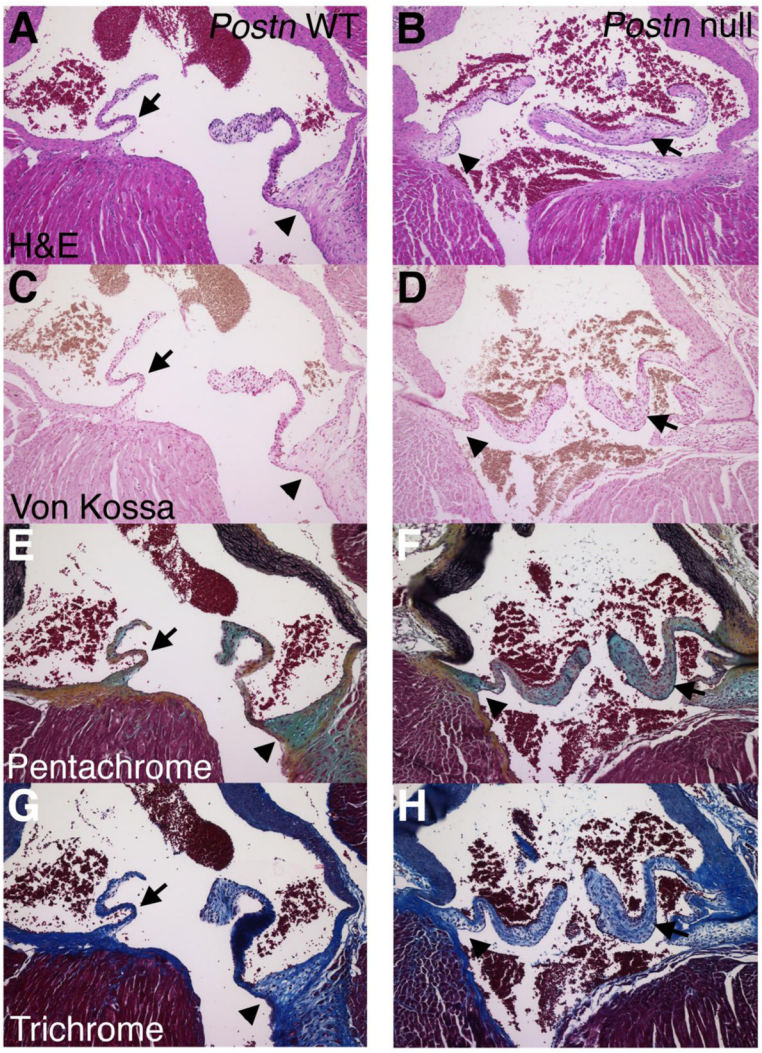

Figure 2. *Periostin* null aortic valve leaflets exhibit thickening of the medial valve region and collagen fiber dysregulation

Postn null mice and wild type controls (WT) were evaluated at 4 months of age by H&E (A,B), von Kossa (C,D), Movat's pentachrome (E,F) and Masson's trichrome (G,H) histological stains. The region of medial thickening and reduced collagen fiber formation is indicated by arrows. The aortic valve hinge region is indicated by arrowheads. Note that no calcification was apparent by von Kossa staining.

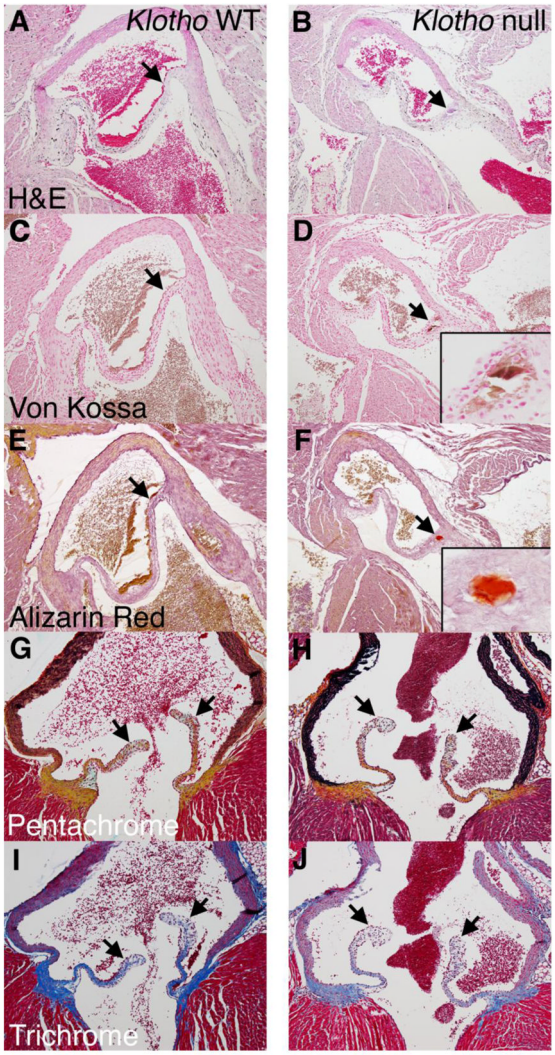

Figure 3. *Klotho* null aortic valve leaflets exhibit nodular calcification at the hinge region

Klotho null mice with premature aging were compared with WT littermate controls at 6 weeks of age. Calcified nodules (arrows) are apparent at the hinge region on the fibrosa side by H&E (A, B), von Kossa (C,D) and Alizarin red (E,F) staining, magnified in insets. Valve stratification and ECM organization are apparently normal by pentachrome (G,H) and trichrome (I,J) staining. The lack of distal thickening is indicated by arrows in G–J.

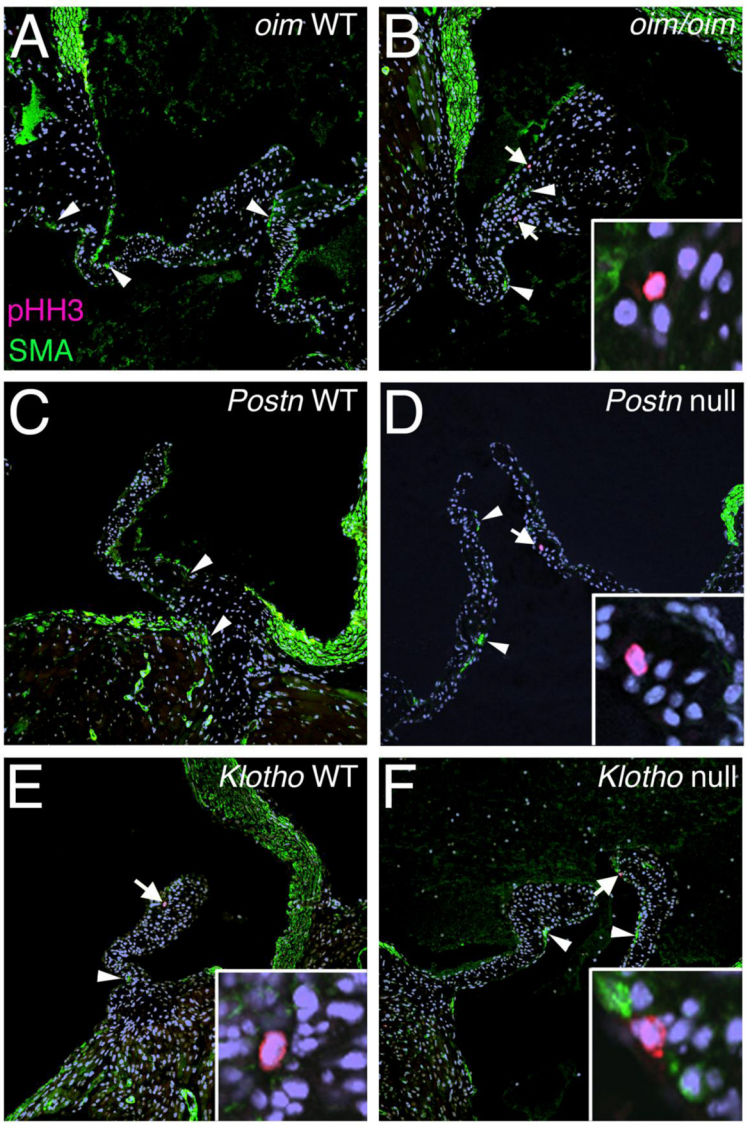

Figure 4. Cell proliferation is increased in the absence of SMA induction in *oim/oim* and *Postn* null aortic valve leaflets

Phospho-Histone H3 (pHH3) immunostaining (red cells, indicated by arrows) was used as an indicator of cell proliferation, and smooth muscle α-actin (SMA) expression (green cells, indicated by arrowheads) also was evaluated in *oim/oim* (A,B), *Postn* null (C,D), and *Klotho* null (E,F) aortic valves in parallel to corresponding controls. Insets in B, D, E, and F, show higher magnification of the pHH3 positive cell (red) in each low magnification panel indicated by an arrow. Note the absence of SMA staining in pHH3 positive cells.

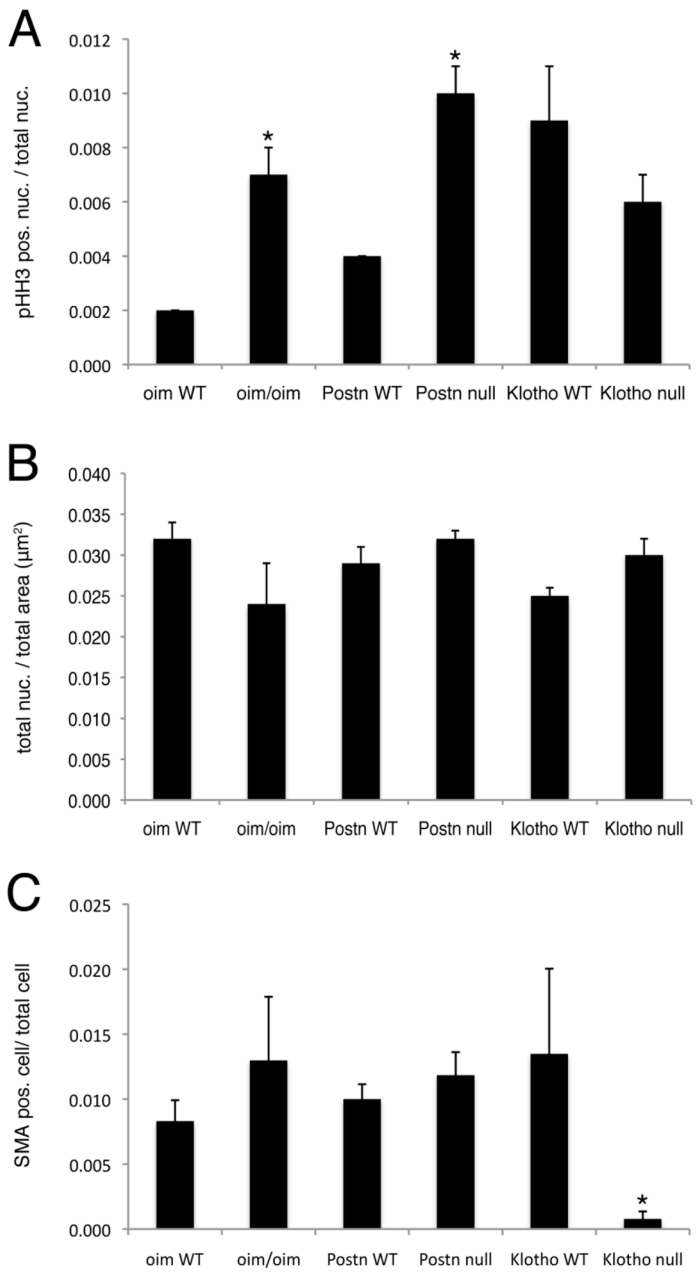

Figure 5. Quantification of cell proliferation, VIC density and SMA expression in mouse models of valve disease

(A) The number of pHH3 positive nuclei/total nuclei in aortic valve leaflets was calculated for 3 independent sections of 3 hearts per genotype. (B) The total number of nuclei per μm^2 of aortic valve leaflet area was calculated for 3 independent sections of 3 hearts per genotype. (C) The number of SMA positive cells/total nuclei in aortic valve leaflets was calculated for 3 independent sections of 3 hearts per genotype. Cohorts of *oim* and *Postn* mice and controls were evaluated at 4 months of age. *Klotho* null mice and WT littermates were evaluated at 6 weeks of age. Statistical significance was determined by paired student's t-test. * is $p \leq 0.05$.

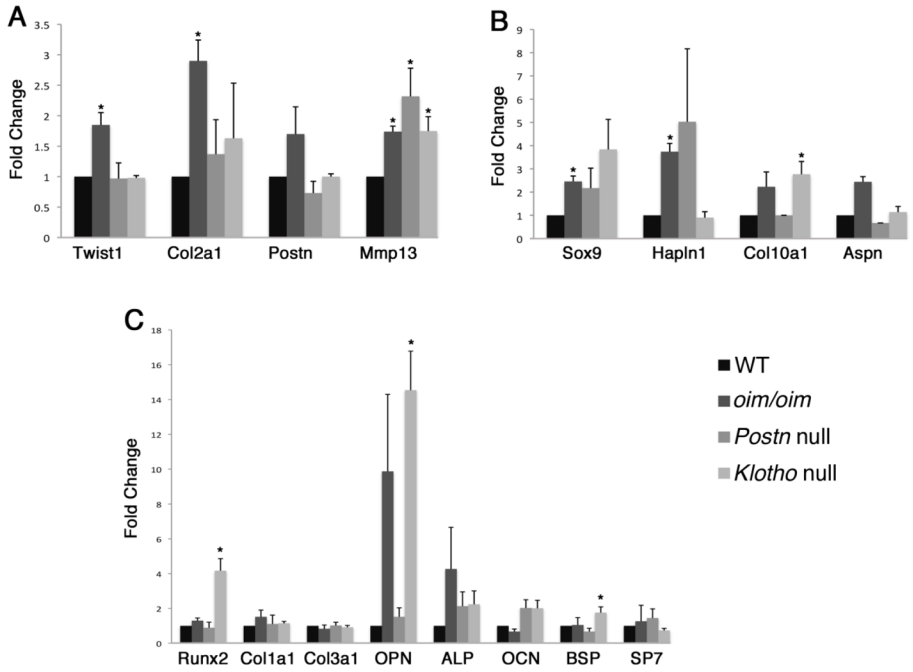

Figure 6. Expression of genes associated with valvulogenesis, chondrogenesis, and osteogenesis are differentially induced in mouse models of valve disease

Expression of indicated genes characteristic of embryonic endocardial cushion (A), cartilage (B), and bone lineages (C) was evaluated in by qRT-PCR of RNA isolated from *oim/oim*, *Postn* null and *Klotho* null aortic valves relative to WT littermate controls for each group. Samples were run in triplicate and expression levels normalized to L7 or B2 microglobulin. Normalized expression values are shown as relative gene expression as compared to the average expression level of the corresponding WT cohort for each individual line, which was set to 1.0. Statistical significance was determined by paired student's t-test. * is $p \leq 0.05$. (Collagen=Col, matrix metalloproteinase=Mmp, Hapln1=hyaluronan and proteoglycan link protein 1, Aspn=Asporin, OPN=osteopontin, ALP=Alkaline phosphatase, OCN=osteocalcin, BSP=Bone Sialoprotein)

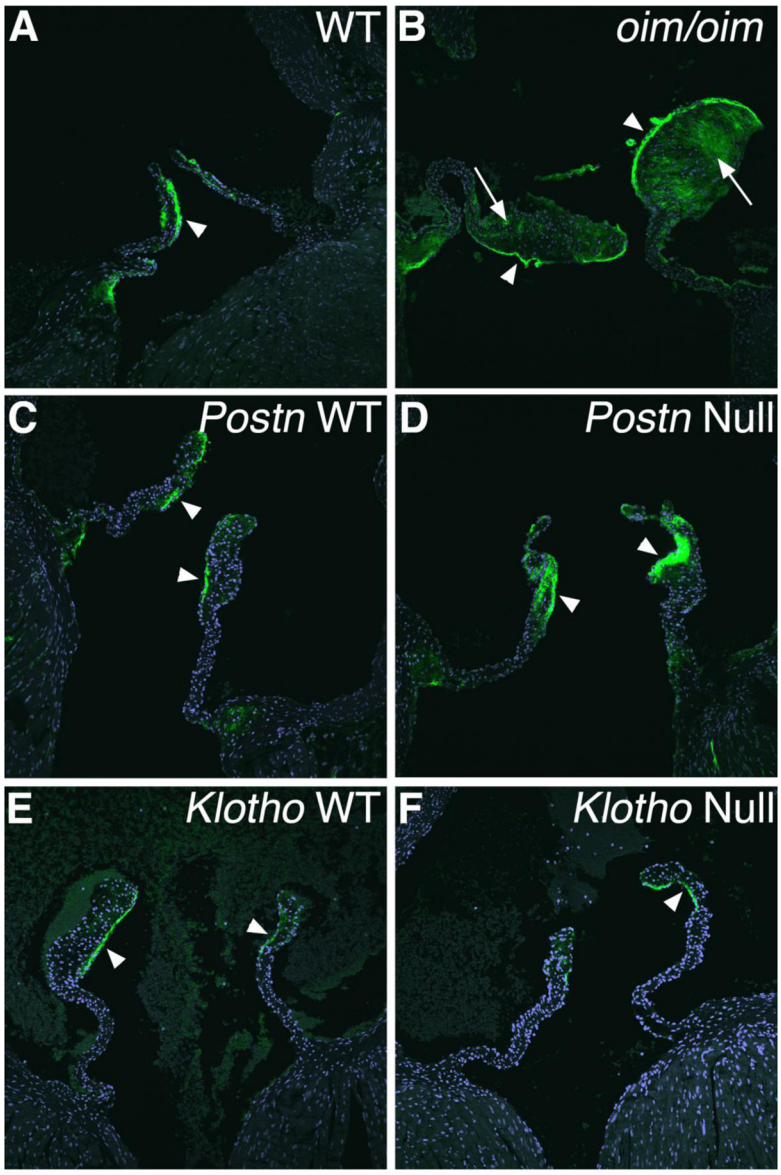

Figure 7. Expression and distribution of Hapln1 protein is abnormal in *oim/oim* and *Postn*-null aortic valves

Expression of Hapln1 protein (green) was detected by immunostaining and confocal microscopy in aortic valves of *oim/oim* (A,B), *Postn* null (C,D), and *Klotho* null (E,F) mice relative to corresponding controls. Increased Hapln1 expression is apparent in the thickened distal regions of the *oim/oim* aortic valve (arrows in B) and in the thickened medial region of *Postn* null aortic valve leaflets (arrowheads in D).

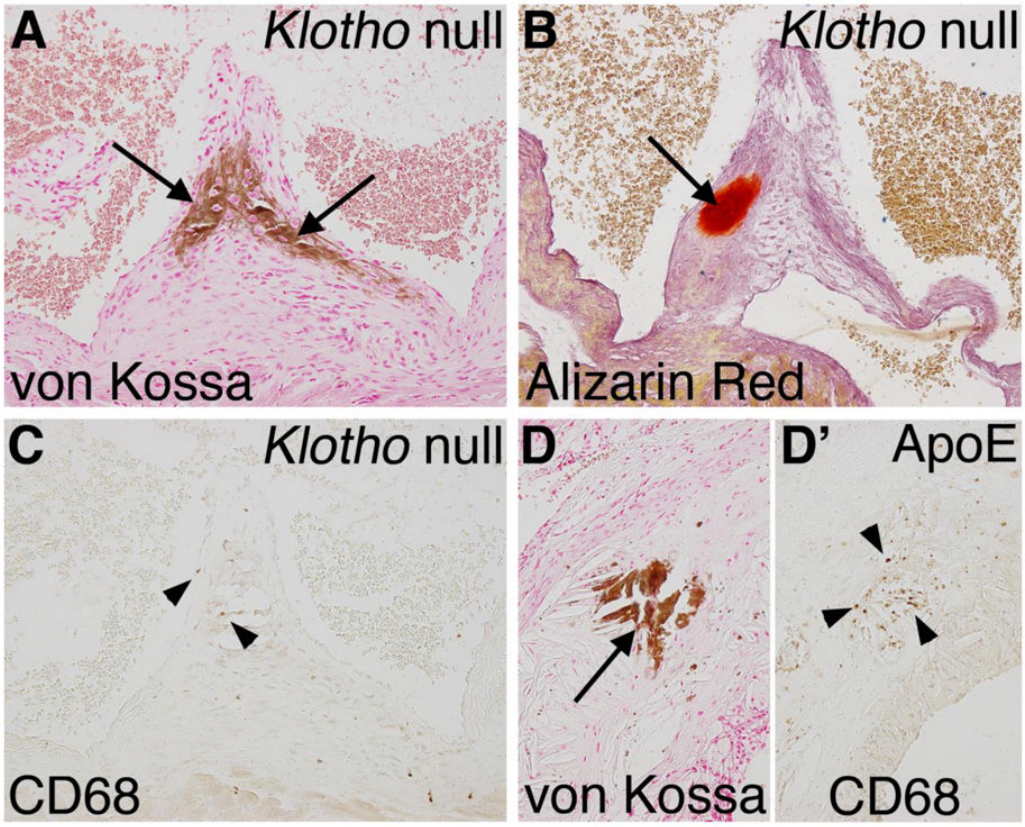

Figure 8. Macrophage infiltration is minimal in calcified lesions of *Klotho* null aortic valve leaflets

Nodular calcification of the aortic valve hinge region (arrows) is apparent in a *Klotho* null aortic valve at 8 weeks of age as detected by von Kossa (A) and Alizarin red (B) staining. Macrophage infiltration was detected by immunoreactivity with CD68 visualized by brown DAB staining in the *Klotho* null valve (C). Sparse and isolated macrophages in the calcified region of the *Klotho* null aortic valve are indicated by arrowheads. High fat fed *ApoE* −/− mice were analyzed for inflammation associated with vascular calcification as a positive control. In the *ApoE* −/− aorta near the aortic root, calcification is apparent by von Kossa staining (D, arrow), in association with extensive inflammation, as indicated by CD68 staining (D′, arrowheads).

Table 1

Morphometric analysis of aortic valve dimensions in mouse models of valve disease.

	WT/*Oim*	***Oim/Oim***	***Postn*+/+**	***Postn*−/−**	***Klotho*+/+**	***Klotho*−/−**
Age	**5 month**	**5 month**	**4 month**	**4 month**	**6–7 wk**	**6–7 wk**
Thickness (μm)						
proximal	103±11[a]	171±14*	135±18	130±10	129±16	155±8
middle	17±1	26±4	15±2	32±4*	24±1	24±1
distal	77±14	157±31*	62±12	75±4	93±14	72±10
Area (mm^2)	.035±.006	.063±.001*	.031±.008	.043±.005	.030±.003	.035±.007

[a] Values are means ± s.e.m.

* $p \leq 0.05$ compared to respective controls, n=3–7 per group.